

Hysteretic upscaled constitutive relationships for vertically integrated porous media flow

Florian Doster · Jan M. Nordbotten ·
Michael A. Celia

Received: date / Accepted: date

Abstract Subsurface two-phase flow in porous media often takes place in reservoirs with a high ratio between the associated lateral and vertical extent and the lateral and vertical flow time scales. This allows for a two-scale approach with effective quantities for two-dimensional horizontal flow equations obtained from reconstructed hydrostatic vertical pressure and saturation distributions. Here, we derive explicit expressions for the two dimensional constitutive relationships for a play-type hysteretic Brooks-Corey capillary pressure function with a pore-size distribution index of 2 and quadratic relative permeabilities. We obtain an explicit hysteretic parametrization for the upscaled capillary pressure function and the upscaled relative permeabilities. The size of the hysteresis loop depends on the ratio between buoyancy and the entry pressure, i.e. it scales with the reservoir height and the ratio between drainage and imbibition capillary pressure. We find that the scaling for the relative permeability is non-monotonic and hysteresis vanishes for both small and large reservoirs.

1 Introduction

Subsurface two-phase flow processes are relevant for various applications ranging from oil recovery, CO₂ storage and soil remediation to water management and risk assessment of contaminants in the vadose zone. These application involve lateral spatial extents on the order of hundreds of meters to tens of kilometers and more. Further, only statistical properties of the relevant parameter fields are known. This renders models for the prediction of fluid and contaminant motion computationally demanding. Often the lateral extent is large compared to the vertical extent and horizontal flow dominates the large scale dynamics. The high density contrast

F. Doster · M.A. Celia
Department of Civil and Environmental Engineering
Princeton University, Princeton, NJ, USA
E-mail: fdoster@princeton.edu

J.M. Nordbotten
Department of Mathematics,
University of Bergen, Bergen, Norway

between the two fluids and moderate horizontal driving forces, e.g. in the vadose zone and in post injection plume migration scenarios in CO₂ storage, yield vertical redistributions on short time scales while lateral redistribution takes much longer. In these cases it is reasonable to assume that the fluids are in vertical equilibrium when the horizontal movement of the fluids is studied. This approximation permits an integration over the vertical direction, reducing the dimensionality of the problem from 3 to 2 and also reducing computational costs significantly. Limits of the vertical equilibrium approximation are investigated in [4]. Consideration of lateral symmetries may eliminate another dimension and even permit analytical solutions [10, 12, 17, 18].

Integration over the vertical extent generates a new set of equations with new parameter functions that depend on the vertical fluid distributions. The vertical equilibrium assumption permits a reconstruction of the vertical distributions from the upscaled variables. In practice, the level of detail which is taken into account in the reconstruction is often very low when the vertical fluid distributions are determined. The most common approach in CO₂-storage-modeling assumes e.g. a complete segregation of the fluids. In this reconstruction scenario – referred to as sharp interface approximation – the lighter fluid occupies the upper part of the vertical domain and the denser fluid the lower part and the vertical position of the interface between the two fluids determines the integrated amount of both fluids. Recently, limitations of the sharp interface approximation have been observed and discussed [19, 16]. The authors observed that the velocity of the tip of CO₂-plumes is overestimated if the capillary transition zone is disregarded. Unfortunately, the consideration of the capillary transition zone requires a numerical calculation of the effective two-dimensional quantities for general rock and fluid properties. Yet, an analytical closed-form expression for the upscaled quantities has been obtained [16] for a specific parametrization of the constitutive parameter functions to improve the understanding and to facilitate analytical studies.

Increasing the level of detail in the reconstruction of the fluid distribution requires choices about additional phenomena to be taken into account. In [19, 16] a unique relation between capillary pressure and saturation has been assumed while experiments clearly show [14] that this relation is hysteretic, i.e. it depends on the process direction and is different whether the amount of one or the other fluid is increased locally. Hence, the equilibrium is not unique and the reconstruction has to account for the process history as well. If the unique capillary transition zone requires numerical calculations of effective quantities, then a process dependent equilibrium does as well. A broad assessment of whether the impact of the hysteretic capillary fringe on upscaled quantities justifies the additional computational costs is in preparation [6]. In this contribution, we take a different approach and incorporate the process dependence of the capillary fringe into the analytical approach of [16] by a play-type hysteresis model [2]. Compromising on the level of detail permits analytical closed-form expressions for the two-dimensional effective quantities, improves our understanding, and allows for further analytical studies.

The article starts with a brief review of the vertically integrated approach to two-phase porous media flow in section 2. In section 3, the upscaled constitutive relations are derived and discussed. The first part, section 3.1, recalls the derivation for a unique, non-hysteretic relation between saturation and capillary pressure from [16] and discusses the possible impact of the hysteresis by comparing results for parametrizations according to the bounding primary drainage and imbibition.

In its second part, section 3.2, the hysteretic upscaled constitutive relationships for secondary processes are calculated. The article closes with a summary in section 4. Further, explicit formulas for the hysteretic quantities are provided in the appendix.

2 Vertically integrated model

In this section, we give a brief review of the equations of the vertically integrated model for porous media flow. We apply several simplifications to focus on the phenomena related to a process-dependent capillary pressure function. For more general derivations we refer to the literature [1, 13, 8, 19, 15].

Consider two immiscible and incompressible fluids and a rigid porous medium under isothermal conditions. The fluids are distinguishable by their wetting properties and we denote one fluid as the wetting fluid w and the other as the non-wetting fluid n . The two fluids have different densities ρ with $\rho_w > \rho_n$. The connected pore space $V_\phi = \phi V$ with porosity ϕ and sample volume V is filled with the two fluids. The fluid volumes are expressed in terms of saturations $s_\alpha = V_\alpha/V_\phi$ with $\alpha \in \{w, n\}$ denoting the corresponding fluid. By this definition

$$s_w + s_n = 1 \quad (1)$$

holds true. Mass conservation for each incompressible fluid requires

$$\frac{\partial \phi s_\alpha}{\partial t} + \nabla \cdot \mathbf{u}_\alpha = 0, \quad (2)$$

when sources are absent. The fluid flow is denoted by \mathbf{u}_α . We assume that the fluid flow is governed by the extended Darcy law

$$\mathbf{u}_\alpha = -k\lambda_\alpha (\nabla p_\alpha - \rho_\alpha \mathbf{g}) \quad (3)$$

with a scalar permeability k a scalar mobility λ_α , the fluid pressure p_α and the gravity acceleration vector \mathbf{g} . The scalar mobility relates to the relative permeability through the viscosity μ_α as $k_{r\alpha} = \lambda_\alpha \mu_\alpha$. The pressures are related by the capillary pressure function

$$p_c = p_n - p_w. \quad (4)$$

We assume, that the capillary pressure and the relative permeability functions are algebraic functions and depend only on saturation and the saturation history. An explicit spatial dependency is neglected for the sake of simplicity. The contribution of other variables and effects such as e.g. specific interfacial area [11], connectivity of the fluids [7], dynamic effects [9] or apparent surface tensions [5] is active ongoing research but not considered here. The equations (1)-(4) form a set of 10 equations for 10 unknowns in three dimensions. They form a closed and solvable system, provided that explicit parametrizations for p_c and $k_{r\alpha}$ and proper initial and boundary conditions are given.

In subsurface flow processes the lateral extent of interest is often substantially larger (hundreds of meters to many kilometers) than the vertical extent (meters to tens of meters). Hence, vertical fluid redistribution often happens on time-scales much shorter than horizontal fluid redistributions and the vertical fluid distribution may be considered to be in hydrostatic equilibrium. A more detailed

estimation and description of involved time-scales is given in [15, 19]. For the sake of clarity, we assume that in the vertical direction the domain - referred to as the reservoir - is bounded by impermeable layers, that the bounds are perpendicular to the gravity vector and that the distance H between them is constant in the whole reservoir. We choose to express terms in a cartesian coordinate system where the z -axis is aligned opposite to gravity. Further, we assume for simplicity that permeability k and porosity ϕ do not vary along the vertical direction.

The aim of the vertical integration is to obtain equations for the horizontal coordinates with variables representative of quantities over the entire vertical extent of the reservoir. We refer to the vertical domain as the fine scale and to the horizontal extent as the coarse scale. Fine-scale quantities are denoted by lower-case letter and coarse-scale quantities by upper-case letters. Equation (3) implies that the pressure gradient in each phase compensates buoyancy in the vertical hydrostatic equilibrium ($u_{\alpha z} = 0$). Hence, the pressure at any vertical position can be obtained by integrating from the value at a reference position. We normalize the z -axis in terms of the reservoir height H with $z = 0$ at the bottom and $z = 1$ at the top of the reservoir and choose the top as reference position

$$P_{\alpha} = p_{\alpha}(z = 1). \quad (5)$$

The reconstructed pressure then is

$$p_{\alpha}(z) = P_{\alpha} + \rho_{\alpha}gH(1 - z). \quad (6)$$

The other coarse-scale quantities are introduced by integrating or averaging the fine scale quantities. We assume a homogeneous system with isothermal and incompressible fluid. We have normalized the vertical axis to the reservoir height and write the equations in dimensionless form. In this particular case, we do not need to bother about the subtle difference and obtain the coarse-scale equivalents of porosity $\Phi = \phi$, density $R_{\alpha} = \rho_{\alpha}$, permeability $K = k$ and viscosity $M_{\alpha} = \mu_{\alpha}$. The spatial dependent quantities are given by

$$S_{\alpha} = \int_0^1 s_{\alpha} dz, \quad (7)$$

$$\mathbf{U}_{\alpha} = \int_0^1 \mathbf{u}_{\alpha||} dz, \quad (8)$$

$$K_{r\alpha} = \int_0^1 k_{r\alpha} dz. \quad (9)$$

We emphasize that the simplifying assumptions have been applied extensively and refer to [15, 19] for a less restrictive formulation. The subscript $||$ denotes the horizontal components and \mathbf{U}_{α} is a two-dimensional vector. With these definitions the integral of eq. (2) over the vertical extent is given by

$$\frac{\partial \Phi S_{\alpha}}{\partial t} + \nabla_{||} \cdot \mathbf{U}_{\alpha} = 0 \quad (10)$$

with the coarse-scale Darcy law

$$\mathbf{U}_{\alpha} = -K \Lambda_{\alpha} \nabla_{||} P_{\alpha} \quad (11)$$

and a two-dimensional horizontal operator $\nabla_{||}$. Also on the coarse-scale the pore volume is conserved

$$S_w + S_n = 1 \quad (12)$$

and the coarse-scale capillary pressure function is defined as

$$P_c(\cdot) = P_n - P_w, \quad (13)$$

where we used the notation (\cdot) to highlight that the arguments of the capillary pressure function are yet to be determined. Note that eqs. (10)-(13) are exact under the given assumptions. Limits of these assumptions have been investigated e.g. in [20,4]. Due to the nonlinear dependence at the fine-scale, the vertical fine-scale saturation distributions $s_w(z; x, y)$ are required to obtain coarse-scale effective parameter functions. Therefore, a reconstruction procedure for s_w has to be provided for a pure coarse-scale model. The assumption of hydrostatic fluid distribution allows for such a reconstruction. From eq. (6) we obtain that the fine-scale capillary pressure has to compensate for buoyancy due to the density difference. From this the fine-scale capillary pressure can be constructed and related to the coarse-scale capillary pressure

$$p_c = P_c - (\rho_w - \rho_n)gH(1 - z). \quad (14)$$

Experimental data for the $p_c(s_w)$ relationship of a well-defined process provides invertible $p_c - s_w$ mappings from which we can reconstruct the vertical saturation distribution for a given P_c and obtain a $P_c - S_w$ relationship with eq. (7). We can then use this relation to obtain the fine-scale saturation distribution $s_w(z; x, y)$ for a given coarse-scale saturation S_w and hence are able to express the coarse-scale relative permeabilities $K_{r\alpha}$ in terms of coarse-scale saturations as well. We will give two simple reconstruction methods now which will serve as bounding reference cases.

Homogeneous saturation distribution

If the reservoir is rather thin it is reasonable to approximate the vertical saturation distribution as constant over the whole vertical extent. From eq. (7)-(9) and (14) we get that in this case, the coarse-scale quantities are identical with the fine-scale quantities.

Sharp interface

If the capillary transition zone is small it may be reasonable to approximate the vertical saturation distribution by assuming that the less dense non-wetting fluid is segregated completely above the denser wetting fluid

$$s_w^s(z, z_I) = \begin{cases} 0, & z > z_I, \\ 1, & z \leq z_I, \end{cases} \quad (15)$$

where z_I is the vertical location of the interface between the two fluids. From eq. (7) we obtain in the dimensionless notation

$$S_w = z_I, \quad (16)$$

and from eq. (9) with eq. (16)

$$K_{rw}(S_w) = S_w k_{rw}(s_w = 1), \quad (17)$$

$$K_{rn}(S_w) = (1 - S_w) k_{rn}(s_w = 0). \quad (18)$$

If the fluids segregate completely and entry pressure is negligible, the pressure difference between the two fluids must vanish at the interface between them. Therefore we obtain from eq. (14)

$$P_c(S_w) = (\rho_w - \rho_n)gH(1 - S_w). \quad (19)$$

Note, that for simplicity we have ignored residual saturations.

3 Explicit hysteretic coarse-scale constitutive relationships

In this section, we will derive and discuss explicit coarse-scale constitutive relationships which take into account the capillary transition zone and the difference in the capillary pressure-saturation relationship for drainage and imbibition processes on the fine-scale. The section is divided into two subsections. The first subsection considers primary processes. Primary processes are an imbibition into a completely dry medium and a drainage of a completely wetting-fluid-saturated medium. The second subsection addresses secondary processes. Secondary processes are an imbibition which starts during a primary drainage and vice versa. An extension of the method to tertiary and higher order processes is straight forward but tedious.

3.1 Primary processes

The capillary transition zone is taken into account by a Brooks-Corey parametrization [3] of the capillary pressure saturation relationship. For the primary drainage and imbibition branch it is given by

$$p_c^\chi(s_w) = p_e^\chi s_w^{-1/\lambda} \quad (20)$$

with $\chi \in \{i, d\}$ indicating imbibition i and drainage d , p_e^χ the corresponding different entry pressures and λ the pore-size distribution index which is assumed to be process independent. We invert this and extend it to capillary pressures below the entry pressure to obtain a function for the saturation depending on capillary pressure

$$\tilde{s}^\chi(p_c) = \begin{cases} \left(\frac{p_c}{p_e^\chi}\right)^{-\lambda}, & \frac{p_c}{p_e^\chi} > 1, \\ 1, & \frac{p_c}{p_e^\chi} \leq 1. \end{cases} \quad (21)$$

As stated in eq. (14) the pressure of each of the phases compensates buoyancy and hence, the capillary pressure has to compensate for the density difference. With the position z_0 at which the fine-scale capillary pressure vanishes we write

$$p_c = (\rho_w - \rho_n)gH(z - z_0). \quad (22)$$

We introduce a dimensionless group similar to the Bond number in free multiphase flow for the ratio between buoyancy and capillary forces

$$B = \frac{(\rho_w - \rho_n)gH}{p_e^d} \quad (23)$$

and the ratio between drainage and imbibition entry pressure

$$\Pi = \frac{p_e^i}{p_e^d}. \quad (24)$$

This allows for determining the saturation distribution in terms of the dimensionless vertical position and the position of the vanishing capillary pressure

$$s^\chi(z, z_0) = \begin{cases} s_1^\chi(z, z_0) = \left[\frac{B}{\Gamma}(z - z_0)\right]^{-\lambda}, & z > \frac{\Gamma}{B} + z_0, \\ s_2^\chi(z, z_0) = 1, & z \leq \frac{\Gamma}{B} + z_0 \end{cases} \quad (25)$$

with $\Gamma = \Pi$ for $\chi = i$ and $\Gamma = 1$ for $\chi = d$. The coarse-scale saturation for a primary process (drainage or imbibition) is determined with respect to z_0 as

$$\begin{aligned} S^\chi(z_0) &= \int_0^1 s^\chi(z; z_0) dz \\ &= \begin{cases} \frac{1}{1-\lambda} \left(\frac{B}{\Gamma}\right)^{-\lambda} \left[(z - z_0)^{1-\lambda}\right]_{z=0}^{z=1}, & z_0 \leq -\frac{\Gamma}{B}, \\ \frac{\Gamma}{B} + z_0 + \frac{1}{1-\lambda} \left(\frac{B}{\Gamma}\right)^{-\lambda} \left[(z - z_0)^{1-\lambda}\right]_{z=\frac{\Gamma}{B}+z_0}^{z=1}, & -\frac{\Gamma}{B} < z_0 < 1 - \frac{\Gamma}{B}, \\ 1, & 1 - \frac{\Gamma}{B} < z_0. \end{cases} \end{aligned} \quad (26)$$

For $\lambda = 2$ this is a quadratic equation of $S_w = S^\chi(z_0)$ in z_0 and hence can be explicitly solved for z_0 and we obtain a relation $z_0 = Z^\chi(S_w)$ for the position at which p_c vanishes

$$Z^\chi(S_w) = \begin{cases} Z_1^\chi(S_w) = \frac{1}{2} \left(1 - \sqrt{1 + \left(\frac{\Gamma}{B}\right)^2 \frac{4}{S_w}}\right), & S_w \leq \frac{\Gamma}{B+\Gamma}, \\ Z_2^\chi(S_w) = \frac{1+S_w}{2} - \frac{\Gamma}{B} - \sqrt{\frac{4\Gamma+B}{4B} - \frac{2\Gamma+B}{2B}S_w + \frac{S_w^2}{4}}, & S_w > \frac{\Gamma}{B+\Gamma}. \end{cases} \quad (27)$$

The second possible solution yields unphysical $z_0 > 1 - \frac{\Gamma}{B}$ with negative contributions to the total saturation.

Figure 1 illustrates reconstructed saturation distributions $s^\chi(z, Z^\chi(S_w))$ for different coarse-scale saturations. The four pairs of profiles represent different branches and their boundaries in eq. (25)-(27). The parameters for the curves in the graph are $B = 1$ and $\Pi = \frac{1}{2}$. For these parameters, the minimum coarse saturation at which the saturation at the bottom is 1 is $S_w = 0.5$ for drainage and $S_w = 1/3$ for imbibition.

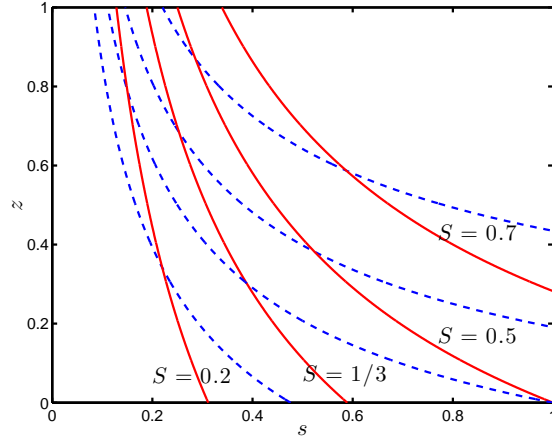


Fig. 1 Reconstructed vertical saturation distributions for drainage (red curves) and imbibition (blue dashed curves) for four different coarse-scale saturations with $B = 1$ and $\Pi = \frac{1}{2}$.

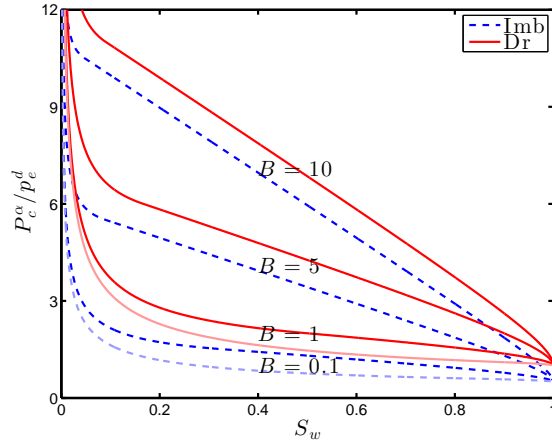


Fig. 2 Coarse capillary pressure function vs. coarse saturation for primary drainage (red solid curves) and imbibition (blue dashed curves) for $B = \{0.1, 1, 5, 10\}$ (from bottom upwards) and $\Pi = \frac{1}{2}$. The curves for $B = 0.1$ are brighter to distinguish them from $B = 1$.

Coarse parameter functions

The macroscopic capillary pressure function is obtained by inserting eq. (22) into eq. (14) and using eq. (27) for z_0 . The result is

$$P_c^X(S_w) = p_e^d B (1 - Z^X(S_w)). \quad (28)$$

Figure 2 illustrates the impact of the ratio of buoyancy and capillary forces and the difference between drainage and imbibition on the coarse-scale capillary pressure. The graph shows that for small values of B , P_c^X is almost independent of B and the fine-scale capillary pressure is recovered. For $B > 1$ buoyancy starts

contributing. For $B \gg 1$ buoyancy is the dominant contribution and $P_c^X(S_w)$ becomes linear in S_w . Further, for $B \rightarrow \infty$ the difference between drainage and imbibition capillary pressure is independent of B and S_w . Proofs for these three statements are given in the appendix in eqs. (80)-(82).

To obtain the coarse-scale relative permeabilities we need to choose fine-scale relative permeabilities. We assume quadratic relative permeabilities since they provide the same qualitative non-linear behavior as relative permeabilities of real materials while still permitting explicit and readable expressions for the coarse parameter functions. They are given by

$$k_{rw}(s_w) = s_w^2, \quad (29)$$

$$k_{rn}(s_w) = (1 - s_w)^2. \quad (30)$$

Often, realistic relative permeabilities are more curved, e.g. higher-order polynomials. Other polynomials are possible as well, e.g. [16], but yield even longer terms for the coarse-scale relative permeabilities. The coarse-scale relative permeabilities are given by

$$\begin{aligned} K_{rw}^X(S_w) &= \int_0^1 k_{rw}(s^X(z, Z^X(S_w))) dz \\ &= \begin{cases} -\frac{1}{3} \left(\frac{B}{\Gamma}\right)^{-4} \left[(z - Z_1^X(S_w))^{-3} \right]_{z=0}^{z=1}, & S_w \leq \frac{\Gamma}{B+\Gamma}, \\ \frac{\Gamma}{B} + Z_2^X(S_w) - \frac{1}{3} \left(\frac{B}{\Gamma}\right)^{-4} \left[(z - Z_2^X(S_w))^{-3} \right]_{z=\frac{\Gamma}{B} + Z_2^X(S_w)}^{z=1}, & S_w > \frac{\Gamma}{B+\Gamma} \end{cases} \end{aligned} \quad (31)$$

for the macroscopic wetting phase relative permeability and

$$\begin{aligned} K_{rn}^X(S_w) &= \int_0^1 k_{rn}(s^X(z, Z^X(S_w))) dz \\ &= \begin{cases} \left[z - \frac{\Gamma^4}{3B^4(z-z_0)^3} + \frac{2\Gamma^2}{B^2(z-z_0)} \right]_{z=1}^{z=0}, & S_w \leq \frac{\Gamma}{B+\Gamma}, \\ \left[z - \frac{\Gamma^4}{3B^4(z-z_0)^3} + \frac{2\Gamma^2}{B^2(z-z_0)} \right]_{z=\frac{\Gamma}{B} + Z_2^X(S_w)}^{z=1}, & S_w > \frac{\Gamma}{B+\Gamma} \end{cases} \end{aligned} \quad (32)$$

for the non-wetting phase.

Figure 3 shows the impact of the ratio of buoyancy and capillary forces and the difference between drainage and imbibition for the coarse-scale relative permeability for the wetting (left) and non-wetting (right) phase. For small B the fine-scale curves are recovered while for large B the relative permeabilities converge to the linear ones of the sharp interface reconstruction. Both limits are process independent. However, for intermediate values $B = \mathcal{O}(1)$ the different vertical saturation distributions lead to different relative permeabilities for drainage and imbibition. Here, the difference between them is moderate but it increases for relative permeabilities with a higher curvature than the quadratic relations. Further, keep in mind that the governing equations for two-phase flow contain the relative permeabilities as products and fractions and hence, moderate alterations may lead to significant changes in the predictions of fluid distributions.

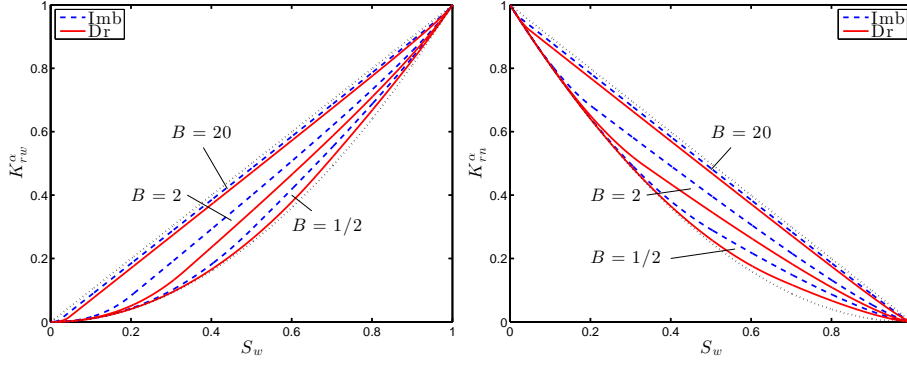


Fig. 3 Coarse wetting phase relative permeability vs. coarse saturation (left figure) and coarse non-wetting phase relative permeability vs. coarse saturation (right figure) for primary drainage (red solid curves) and primary imbibition (blue dashed curves) for $B = \{1/2, 2, 20\}$ (from bottom upwards) and $\Pi = \frac{1}{2}$. For reference, the fine-scale quadratic and the linear sharp interface relative permeabilities are shown as black dotted curves.

3.2 Secondary processes

In the previous section we have discussed the analytic reconstruction for a primary drainage and a primary imbibition. We use now a simple hysteresis model to extend the reconstruction to a secondary imbibition and a secondary drainage. In a secondary imbibition (*di*), the reservoir is imbibed after it has been drained to a saturation S^t with S^t referred to as the turning saturation. The corresponding equilibrium profile is $s^d(z, z^t)$ with $z^t = Z^d(S^t)$. An imbibition takes place when the point of vanishing capillary pressure z_0 (this corresponds to the water table up to a constant Γ/B) is increased with respect to the turning position z^t because this decreases the capillary pressure at each vertical position z in the reservoir. In a secondary drainage (*id*), the reservoir is drained after it has been imbibed to a saturation S^t . The corresponding equilibrium profile is $s^i(z, z^t)$ with $z^t = Z^i(S^t)$. The reservoir is drained if the point of vanishing capillary pressure z_0 is decreased with respect to the turning position z^t because this increases the capillary pressure everywhere along the z -axis.

Differences between drainage and imbibition are considered in the capillary pressure–saturation relation according to a play-type hysteresis model [2]. After the process direction has changed, the saturation is not changed until the capillary pressure is equal to the value of the primary capillary pressure–saturation relationship of the current process. Only then does the saturation decrease (for a drainage process) and increase (for an imbibition process). The fine-scale saturation for a drainage after an imbibition can be written as follows,

$$s^{id}(z, z_0, z^t) = \begin{cases} s^i(z, z^t), & p_c^d \left[s^i(z, z^t) \right] > p_c^d \left[s^d(z, z_0) \right], \\ s^d(z, z_0), & p_c^d \left[s^i(z, z^t) \right] \leq p_c^d \left[s^d(z, z_0) \right]. \end{cases} \quad (33)$$

Similarly, the saturation for an imbibition after a drainage is

$$s^{di}(z, z_0, z^t) = \begin{cases} s^i(z, z_0), & p_c^i \left[s^d(z, z^t) \right] < p_c^i \left[s^i(z, z_0) \right], \\ s^d(z, z^t), & p_c^i \left[s^d(z, z^t) \right] \geq p_c^i \left[s^i(z, z_0) \right]. \end{cases} \quad (34)$$

The saturation distribution at the turning point z^t is monotonic in the considered parameterization and so are the capillary pressure relationships. Hence, there is only one position $z^*(z_0, z^t)$ along the z -axis which separates a drainage branch from an imbibition branch. In the considered parameterization of the capillary pressure (20), the entry pressure for drainage p_e^d and imbibition p_e^i are process dependent but the pore-size distribution index $\lambda = 2$ is independent of the process. By inserting the first case of eq. (25) and eq. (20) into the branching inequalities in eq. (33) and (34) we obtain

$$z^*(z_0, z^t) = \begin{cases} \frac{1}{1-\Pi} (z^t - \Pi z_0), & id : z_0 < z^t, \\ \frac{1}{1-\Pi} (z_0 - \Pi z^t), & di : z_0 > z^t. \end{cases} \quad (35)$$

The separating position moves upwards in the reservoir for a secondary process because the saturation decreases with height and the capillary pressure increases for decreasing saturations. This is independent from whether a drainage after an imbibition (*id*) or an imbibition after a drainage (*di*) is considered. To observe that explicitly, compare z^* for a diminishing z_0 in the first, and an increasing z_0 in the second line of eq. (35). The second case in eq. (25) provides a threshold for the absolute difference $|z_0 - z^t|$ below which z^* is not uniquely defined. This will be discussed below when the specific expressions for secondary drainage and imbibition are given. Two values $z^* = 0$ (bottom of the reservoir) and $z^* = 1$ (top of the reservoir) are of specific interest because they define bounds of the hysteresis loop and outside that interval the parametrization is independent of the process history. If $z^* < 0$ the difference $|z_0 - z^t|$ is too small to induce a change of saturation in the reservoir. Hence, $z_0 < z^t/\Pi$ for *id* and $z_0 > \Pi z^t$ for *di*. Because of the second case in eq. (25) the difference has to be at least $(1-\Pi)/B$ and hence a saturation change is observed for

$$z^* = 0 \Rightarrow \begin{cases} z_0 < \min \left(\frac{z^t}{\Pi}, z^t - \frac{1-\Pi}{B} \right), & id : z_0 < z^t, \\ z_0 > \max \left(\Pi z^t, z^t + \frac{1-\Pi}{B} \right), & di : z_0 > z^t. \end{cases} \quad (36)$$

If $z^* > 1$ the difference $|z_0 - z^t|$ is big enough so that in the whole reservoir the current process is taking place and the turning point no longer has an influence on the saturation distribution. Because of the monotonicity of p_c^x the branching in eq. (25) has no impact on the solution and

$$z^* = 1 \Rightarrow \begin{cases} z_0 < \frac{z^t - (1-\Pi)}{\Pi}, & id : z_0 < z^t, \\ z_0 > 1 - \Pi + \Pi z^t, & di : z_0 > z^t. \end{cases} \quad (37)$$

The points of vanishing capillary pressure at the fine-scale correspond to the coarse-scale capillary pressure up to a linear transformation (28). A relation between the coarse saturation S_w and the coarse capillary pressure P_c is obtained by integrating the fine-scale saturation distribution (33) and (34) over the vertical extent. The branching in eq. (25)-(27) leads to various cases in this relationship

as well. Further, often the coarse-scale equations are expressed in terms of saturations and hence the inverted relationship P_c of S_w is of interest. This requires some explicit calculations which are different for secondary drainage and imbibition and are discussed in separate sections.

3.2.1 Secondary imbibition (di)

In eq. (36) and (37) the lower \bar{z}_ℓ^{di} and the upper \bar{z}_u^{di} bound of the transition zone are given as

$$\bar{z}_\ell^{di}(z^t) = \begin{cases} \Pi z^t, & z^t \leq -\frac{1}{B}, \\ z^t + \frac{1-\Pi}{B}, & z^t > -\frac{1}{B}, \end{cases} \quad (38)$$

$$\bar{z}_u^{di}(z^t) = 1 - \Pi + \Pi z^t \quad (39)$$

and hence the coarse-scale saturation is

$$S^{di}(z_0, z^t) = \begin{cases} S^d(z_0), & z_0 < z^t, \\ S^d(z^t), & z^t \leq z_0 < \bar{z}_\ell^{di}, \\ \int_0^1 s^{di} dz, & \bar{z}_\ell^{di} \leq z_0 < \bar{z}_u^{di}, \\ S^i(z_0), & \bar{z}_u^{di} \leq z_0. \end{cases} \quad (40)$$

Note that for $s^{di} = s^{di}(z; z_0, z^t)$, $\bar{z}_\ell^{di} = \bar{z}_\ell^{di}(z^t)$ and $\bar{z}_u^{di} = \bar{z}_u^{di}(z^t)$ the arguments have been omitted for clarity. We define the largest z for which $s^i(z, z_0) = 1$ holds as

$$\bar{z}_1^{di}(z_0) = \frac{\Pi}{B} + z_0. \quad (41)$$

The integral for the transition from a displacement, where only part of the column is imbibed, to a displacement, where the whole column is imbibed, is given by

$$\begin{aligned} \int_0^1 s^{di} dz &= \int_0^{z^*} s^i(z; z_0) dz + \int_{z^*}^1 s^d(z; z^t) dz \\ &= \begin{cases} \int_0^{z^*} s_1^i(z; z_0) dz + \int_{z^*}^1 s_1^d(z; z^t) dz, & \bar{z}_1^{di} \leq 0 \\ \int_0^{\bar{z}_1^{di}} dz + \int_{\bar{z}_1^{di}}^{z^*} s_1^i(z; z_0) dz + \int_{z^*}^1 s_1^d(z; z^t) dz, & \bar{z}_1^{di} > 0 \end{cases} \\ &= \begin{cases} S_1^{di} = -\left(\frac{B}{\Pi}\right)^{-2} \left[\frac{1}{z-z_0}\right]_0^{z^*} - B^{-2} \left[\frac{1}{z-z^t}\right]_{z^*}^1, & \bar{z}_1^{di} \leq 0, \\ S_2^{di} = \bar{z}_1^{di} - \left(\frac{B}{\Pi}\right)^{-2} \left[\frac{1}{z-z_0}\right]_{\bar{z}_1^{di}}^{z^*} - B^{-2} \left[\frac{1}{z-z^t}\right]_{z^*}^1, & \bar{z}_1^{di} > 0. \end{cases} \quad (42) \end{aligned}$$

Note that for $s^{di} = s^{di}(z; z_0, z^t)$, $S_1^{di} = S_1^{di}(z_0, z^t)$, $S_2^{di} = S_2^{di}(z_0, z^t)$, $z^* = z^*(z_0, z^t)$ and $\bar{z}_1^{di} = \bar{z}_1^{di}(z_0)$ the arguments have again been omitted for clarity.

To obtain a relation for the point of vanishing capillary pressure in terms of coarse-scale saturations, eq. (40) has to be inverted with respect to z_0 and the

turning point has to be expressed in terms of the turning saturation $S^t = S^d(z^t)$. The inversion is algebraically possible because the equations are quadratic (since $z^*(z_0, z^t)$ is linear with respect to z_0). However, the expressions are long and new branches are induced because of the branches in eqs. (26) and (27). For the sake of readability, we give the explicit expressions for the inverted quantities in the appendix. Here, we will resolve the branches and stick to representative notations.

The first and the last case in eq. (40) have been inverted already for the primary processes and the second case is trivial since it does not depend on z_0 but only defines S^t . Hence, only the two functions $S_1^{di}(z_0, z^t), S_2^{di}(z_0, z^t)$ in eq. (42) have to be inverted using $z^t = Z_1^d(S^t)$ and $z^t = Z_2^d(S^t)$. Note that the combination Z_2^d and S_1^{di} is not possible because saturations for the imbibition are equal or larger than the drainage ones throughout the whole z -axis. We obtain

$$Z_1^{di}(S_w, S^t) = \left\{ z_0 \mid S_1^{di} \left[z_0, Z_1^d(S^t) \right] = S_w \right\}, \quad (43)$$

$$Z_2^{di}(S_w, S^t) = \left\{ z_0 \mid S_2^{di} \left[z_0, Z_1^d(S^t) \right] = S_w \right\}, \quad (44)$$

$$Z_3^{di}(S_w, S^t) = \left\{ z_0 \mid S_2^{di} \left[z_0, Z_2^d(S^t) \right] = S_w \right\}. \quad (45)$$

These are quadratic equations and are solvable algebraically with two branches of which one is omitted because of negative saturations and physically inconsistent z_0 . The explicit expressions are given in the appendix in eqs. (83)-(85).

Figure 4 illustrates different characteristic saturation distributions. For a small turning saturation, e.g. $S^t = 0.1$, z^* becomes greater than one before a region with $s_w = 1$ appears in the column. The complete transition relation is therefore determined by $Z_1^{di}(S_w, S^t)$. For $S^t = 0.25$, a region which is saturated by the wetting phase appears during the transition. The transition relation is hence given by $Z_1^{di}(S_w, S^t)$ for small saturations S_w and by $Z_2^{di}(S_w, S^t)$ for larger saturations. For $S^t = 0.6$, there is always a wetting-phase-saturated domain and the complete transition relation is determined by $Z_3^{di}(S_w, S^t)$.

The bounds also have to be expressed in saturations. The lower bound

$$\bar{S}_\ell^{di}(S^t) = S^t \quad (46)$$

is trivial. The upper bound has three branches according to the three cases illustrated in Fig. 4. These consist of either using $Z_1^d(S^t)$ or $Z_2^d(S^t)$ to obtain z^t from S^t and $S_1^i(\bar{z}_u^{di})$ or $S_2^i(\bar{z}_u^{di})$ to obtain \bar{S}_u^{di} from \bar{z}_u^{di} of eq. (39). Again, the combination $Z_2^d - S_1^i$ is not possible. Explicitly, this is given by

$$\bar{S}_u^{di}(S^t) = \begin{cases} S_1^i \left(\bar{z}_u^{di} \left[Z_1^d(S^t) \right] \right), & S^t < \bar{S}_1^{di}, \\ S_2^i \left(\bar{z}_u^{di} \left[Z_1^d(S^t) \right] \right), & \bar{S}_1^{di} \leq S^t \leq \frac{1}{1+B}, \\ S_2^i \left(\bar{z}_u^{di} \left[Z_2^d(S^t) \right] \right), & S^t > \frac{1}{1+B}, \end{cases} \quad (47)$$

where \bar{S}_1^{di} defines the turning saturation below which the transition from primary drainage to primary imbibition happens before \bar{z}_1^{di} enters the reservoir. Hence, it is given as

$$\begin{aligned} \bar{S}_1^{di} : \quad & z^* \left[Z_1^i \left(\frac{\Pi}{\Pi + B} \right), Z_1^d(\bar{S}_1^{di}) \right] = 1 \\ \Rightarrow \bar{S}_1^{di} = & \frac{\Pi^2}{B^2(1 - \Pi) + B(2 - \Pi)\Pi + \Pi^2} \end{aligned} \quad (48)$$

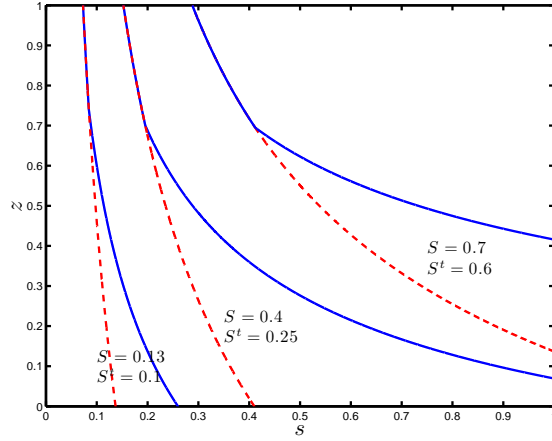


Fig. 4 Reconstructed vertical saturation distributions for a secondary imbibition (blue curves) and the turning profile (red dashed curves) for three different coarse-scale saturation-pairs (S_w, S^t) , $B = 1$ and $\Pi = \frac{1}{2}$.

For intermediate turning saturations (second case in eq. (47)) the position \bar{z}_1^{di} passes 0 in the transition zone. The corresponding saturation is

$$\bar{S}_m^{di}(S^t) = S_1^{di} \left[-\frac{\Pi}{B}, Z_1^d(S^t) \right]. \quad (49)$$

Finally, we can express the position of the vanishing capillary pressure in terms of saturations as

$$Z^{di}(S_w, S^t) = \begin{cases} Z^d(S_w), & S_w < \bar{S}_\ell^{di}(S^t), \\ Z_T^{di}(S_w, S^t), & \bar{S}_\ell^{di}(S^t) \leq S_w < \bar{S}_u^{di}(S^t), \\ Z^i(S_w), & \bar{S}_u^{di}(S^t) \leq S_w, \end{cases} \quad (50)$$

where the transition zone function is given by

$$Z_T^{di}(S_w, S^t) = \begin{cases} Z_1^{di}(S_w, S^t), & S^t < \bar{S}_1^{di}, \\ \begin{cases} Z_1^{di}(S_w, S^t), & S_w < \bar{S}_m^{di}(S^t), \\ Z_2^{di}(S_w, S^t), & S_w \geq \bar{S}_m^{di}(S^t), \end{cases} & \bar{S}_1^{di} \leq S^t < \frac{1}{1+B}, \\ Z_3^{di}(S_w, S^t), & \frac{1}{1+B} \leq S^t. \end{cases} \quad (51)$$

The jump $\Delta z^{di} = \bar{z}_\ell^{di}(z^t) - z^t$ of the vanishing capillary pressure position in terms of the turning saturation is of interest because that is what carries to the coarse-scale from the jump of the fine-scale play-type hysteresis model. From eq. (38) we obtain

$$\Delta z^{di}(S^t) = \begin{cases} -(1 - \Pi)Z_1^d(S^t), & S^t \leq \frac{1}{B+1}, \\ \frac{1-\Pi}{B}, & S^t > \frac{1}{B+1}. \end{cases} \quad (52)$$

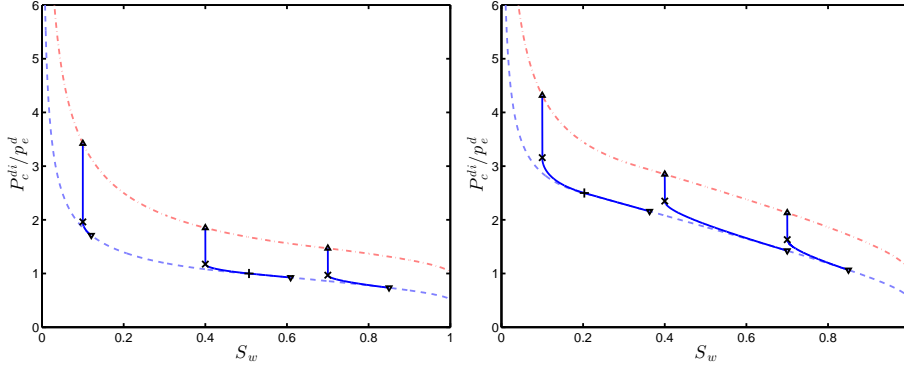


Fig. 5 The transition part (solid blue curves) of the coarse-scale capillary pressure – coarse-scale saturation relation for a secondary imbibition for example turning saturations $S^t = \{0.1, 0.4, 0.7\}$, $B = \frac{1}{2}$ (left) and $B = 2$ (right) and $\Pi = \frac{1}{2}$. The bounding primary imbibition curves are shown as dashed blue and the bounding primary drainage curves as dash-dotted red curves. The values $P_c^d(S^t)$ are shown as upwards pointing triangles, the values $P_c^{di}(S^t, S^t)$ as crosses, $P_c^{di}(\bar{S}_u^{di}(S^t), S^t)$ as downwards pointing triangles and $P_c^{di}(\bar{S}_m^{di}(S^t), S^t)$ as pluses.

With this, we can study how the fraction of the jump after the turning points compares to the difference between the main loops, and obtain from eq. (28) and eq. (82)

$$\lim_{B \rightarrow \infty} \frac{\Delta z^{di}(S^t)}{Z_2^d(S^t) - Z_2^i(S^t)} = \frac{1}{2}. \quad (53)$$

Coarse parameter functions

The capillary pressure is obtained similar to eq. (28) and is given by

$$P_c^{di}(S_w, S^t) = p_e^d B \left(1 - Z^{di}(S_w, S^t)\right). \quad (54)$$

Figure 5 illustrates the relationship for $B = \frac{1}{2}$ (left) and $B = 2$ (right). The bounding primary curves are shown as red dash-dotted (drainage) and blue dashed (imbibition) curves. The transition zone is shown for three examples turning saturations as blue solid curves. Starting from the turning saturation (upwards pointing triangle) on the primary drainage curve, the capillary pressure decreases without a change in saturation until the value $P_c^{di}(S^t, S^t)$ is reached (crosses). The jump spans a smaller fraction of the difference between the bounding curves for $B = \frac{1}{2}$ than for $B = 2$ and illustrates that for $B \rightarrow 0$ the fine-scale play-type is recovered (fraction of the jump is 1 and there is no transition zone) and for $B \rightarrow \infty$ the fraction is $\frac{1}{2}$. The transition curve approaches the primary imbibition curve and hits it at $\bar{S}_u^{di}(S^t)$ (downwards pointing triangles). If the transition zone includes a transition from Z_1^{di} to Z_2^{di} at \bar{S}_m^{di} (this is the case for $S^t = 0.4$ at $B = \frac{1}{2}$ and $S^t = 0.1$ at $B = 2$) the corresponding value $P_c^{di}(\bar{S}_m^{di})$ is shown by a plus.

The relative permeabilities are obtained similar to the coarse-scale saturation in terms of z_0 and z^t . Since we have explicit expressions for $z_0 = Z^{di}(S_w, S^t)$ and $z^t = Z^d(S^t)$, it is also straight forward to obtain relative permeabilities in terms

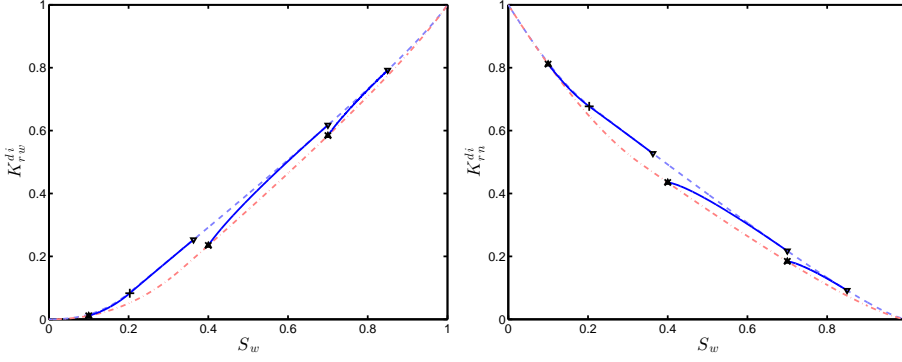


Fig. 6 The transition part (solid blue curves) of the coarse-scale wetting relative permeability (left) – and non-wetting relative permeability (right) – coarse-scale saturation relation for a secondary imbibition for example turning saturations $S^t = \{0.1, 0.4, 0.7\}$, $B = 2$ and $\Pi = \frac{1}{2}$. The bounding primary imbibition curves are shown as dashed blue and the bounding primary drainage curves as dash-dotted red curves. The values $K_{r\alpha}^d(S^t)$ are shown as upwards pointing triangles, the coinciding values $K_{r\alpha}^{di}(S^t, S^t)$ as crosses, $K_{r\alpha}^{di}(\bar{S}_u^{di}(S^t), S^t)$ as downwards pointing triangles and $K_{r\alpha}^{di}(\bar{S}_m^{di}(S^t), S^t)$ as pluses.

of S_w and S^t . They are given by

$$K_{r\alpha}^{di}(S_w, S^t) = \begin{cases} K_{r\alpha}^d(S_w), & S_w < \bar{S}_\ell^{di}(S^t), \\ K_{r\alpha T}^{id}(S_w, S^t), & \bar{S}_\ell^{di}(S^t) \leq S_w < \bar{S}_u^{di}(S^t), \\ K_{r\alpha}^i(S_w), & \bar{S}_u^{di}(S^t) \leq S_w, \end{cases} \quad (55)$$

where the transition-zone relative permeability is given by

$$K_{r\alpha T}^{id}(S_w, S^t) = \begin{cases} K_{r\alpha 1}^{di}(S_w, S^t), & S^t < \bar{S}_1^{di}, \\ \begin{cases} K_{r\alpha 1}^{di}(S_w, S^t), & S_w < \bar{S}_m^{di}(S^t), \\ K_{r\alpha 2}^{di}(S_w, S^t), & S_w \geq \bar{S}_m^{di}(S^t), \end{cases} & \bar{S}_1^{di} \leq S^t < \frac{1}{1+B}, \\ K_{r\alpha 3}^{di}(S_w, S^t), & \frac{1}{1+B} \leq S^t \end{cases} \quad (56)$$

with the same branches as in eq. (50) and (51) and $\alpha \in \{w, n\}$. These branches yield integration boundaries for the upscaling procedure. Explicitly, the integrals are given by

$$K_{r\alpha 1}^{di}(S_w, S^t) = \int_0^{z^*} k_{r\alpha} \left(s_1^i \left[z, Z_1^{di}(S_w, S^t) \right] \right) dz + \int_{z^*}^1 k_{r\alpha} \left(s_1^d \left[z, Z_1^d(S^t) \right] \right) dz, \quad (57)$$

where the arguments of $z^* = z^* [Z_1^{di}(S_w, S^t), Z_1^d(S^t)]$ have been omitted and

$$\begin{aligned} K_{r\alpha 2}^{di}(S_w, S^t) &= \bar{z}_1^{di} k_{r\alpha}(1) + \int_{\bar{z}_1^{di}}^{z^*} k_{r\alpha}(s_1^i [z, Z_2^{di}(S_w, S^t)]) dz \\ &+ \int_{z^*}^1 k_{r\alpha}(s_1^d [z, Z_1^d(S^t)]) dz \end{aligned} \quad (58)$$

where the arguments of $z^* = z^* [Z_2^{di}(S_w, S^t), Z_1^d(S^t)]$ and $\bar{z}_1^{di} = \bar{z}_1^{di} [Z_2^{di}(S_w, S^t)]$ have been omitted and

$$\begin{aligned} K_{r\alpha 3}^{di}(S_w, S^t) &= \bar{z}_1^{di} k_{r\alpha}(1) + \int_{\bar{z}_1^{di}}^{z^*} k_{r\alpha}(s_1^i [z, Z_3^{di}(S_w, S^t)]) dz \\ &+ \int_{z^*}^1 k_{r\alpha}(s_1^d [z, Z_2^d(S^t)]) dz \end{aligned} \quad (59)$$

where the arguments of $z^* = z^* [Z_3^{di}(S_w, S^t), Z_2^d(S^t)]$ and $\bar{z}_1^{di} = \bar{z}_1^{di} [Z_3^{di}(S_w, S^t)]$ have been omitted.

Figure 6 illustrates the relative permeability for the wetting phase (left) and the non-wetting phase (right) for a secondary imbibition with $B = 2$. The bounding primary curves are shown as red dash-dotted (drainage) and blue dashed (imbibition) curves. The transition zone is shown for three example turning saturations as blue solid curves. There is no jump similar to the capillary pressure curve and the values $K_{r\alpha}^d(S^t)$ and $K_{r\alpha}^{di}(\bar{S}_\ell^{di}(S^t), S^t)$ coincide. Crosses and upwards pointing triangles are hence on top of each other. The transition leaves the drainage curve with a substantial kink and approaches the primary imbibition curve smoothly and hits it at $\bar{S}_u^{di}(S^t)$ (downwards pointing triangles). The transition zone includes a transition from Z_1^{di} to Z_2^{di} at \bar{S}_m^{di} for $S^t = 0.1$ and the corresponding values $K_{rw}^{di}(\bar{S}_m^{di})$ and $K_{rn}^{di}(\bar{S}_m^{di})$ are shown by pluses.

3.2.2 Secondary drainage (*id*)

In eq. (36) and (37) the lower and the upper bound of the transition zone are given as

$$\bar{z}_u^{id}(z^t) = \begin{cases} \frac{z^t}{\Pi}, & z^t \leq -\frac{\Pi}{B}, \\ z^t - \frac{1-\Pi}{B}, & z^t > -\frac{\Pi}{B}, \end{cases} \quad (60)$$

$$\bar{z}_\ell^{id}(z^t) = \frac{z^t - (1 - \Pi)}{\Pi}. \quad (61)$$

The notation is reversed with respect to the secondary imbibition *di* because z_0 is lowered during a drainage but $z^* = 0$ is still reached before $z^* = 1$ during the

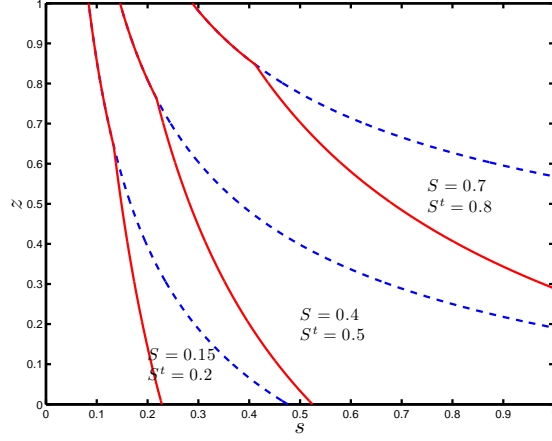


Fig. 7 Reconstructed vertical saturation distributions for a secondary drainage (red curves) and the turning profile (blue dashed curves) for three different coarse-scale saturation-pairs (S_w, S^t) , $B = 1$ and $\Pi = \frac{1}{2}$.

displacement. The coarse-scale saturation here is

$$S^{id}(z_0, z^t) = \begin{cases} S^d(z_0), & z_0 < \bar{z}_\ell^{id}, \\ \int_0^1 s^{id} dz, & \bar{z}_\ell^{id} \leq z_0 < \bar{z}_u^{id}, \\ S^i(z^t), & \bar{z}_u^{id} \leq z_0 < z^t, \\ S^i(z_0), & z^t \leq z_0. \end{cases} \quad (62)$$

Note that for $s^{id} = s^{id}(z; z_0, z^t)$, $\bar{z}_\ell^{id} = \bar{z}_\ell^{id}(z^t)$ and $\bar{z}_u^{id} = \bar{z}_u^{id}(z^t)$ the arguments have been omitted for clarity. We define the largest z for which $s^d(z, z_0) = 1$ as

$$\bar{z}_1^{id}(z_0) = \frac{1}{B} + z_0. \quad (63)$$

The integral for the transition from a displacement where only part of the column is drained to a displacement where the whole column is drained is similar to (42) and given by

$$\begin{aligned} \int_0^1 s^{id} dz &= \int_0^{z^*} s^d(z; z_0) dz + \int_{z^*}^1 s^i(z; z^t) dz \\ &= \begin{cases} S_1^{id} = -B^{-2} \left[\frac{1}{z-z_0} \right]_0^{z^*} - \left(\frac{B}{\Pi} \right)^{-2} \left[\frac{1}{z-z^t} \right]_{z^*}^1, & \bar{z}_1^{id} \leq 0, \\ S_2^{id} = \bar{z}_1^{id} - B^{-2} \left[\frac{1}{z-z_0} \right]_{\bar{z}_1^{id}}^{z^*} - \left(\frac{B}{\Pi} \right)^{-2} \left[\frac{1}{z-z^t} \right]_{z^*}^1, & \bar{z}_1^{id} > 0. \end{cases} \end{aligned} \quad (64)$$

Note that for $s^{id} = s^{id}(z; z_0, z^t)$, $S_1^{id} = S_1^{id}(z_0, z^t)$, $S_2^{id} = S_2^{id}(z_0, z^t)$, $z^* = z^*(z_0, z^t)$ and $\bar{z}_1^{id} = \bar{z}_1^{id}(z_0)$ the arguments have again been omitted for clarity.

Again, we invert eq. (62) with respect to z_0 and express the turning point in terms of the turning saturation $S^t = S^i(z^t)$ to obtain a relation for the point

of vanishing capillary pressure in terms of coarse-scale saturations. Explicit expressions for the inverted quantities are once more moved to the appendix and representative notations are used here.

The two new functions for secondary drainage are $S_1^{id}(z_0, z^t)$ and $S_2^{id}(z_0, z^t)$ in eq. (64) and are inverted using $z^t = Z_1^i(S^t)$ and $Z_2^i(S^t)$. Note that here the combination $Z_1^i - S_2^{id}$ is not possible. We obtain

$$Z_1^{id}(S_w, S^t) = \left\{ z_0 \left| S_1^{id} \left[z_0, Z_1^i(S^t) \right] = S_w \right. \right\}, \quad (65)$$

$$Z_2^{id}(S_w, S^t) = \left\{ z_0 \left| S_1^{id} \left[z_0, Z_2^i(S^t) \right] = S_w \right. \right\}, \quad (66)$$

$$Z_3^{id}(S_w, S^t) = \left\{ z_0 \left| S_2^{id} \left[z_0, Z_2^i(S^t) \right] = S_w \right. \right\}. \quad (67)$$

These are again quadratic equations and one of the solutions is discarded because of negative saturations and physically inconsistent z_0 . The explicit expressions are given in the appendix in eqs. (86)-(88).

Figure 7 illustrates different characteristic saturation distributions. If the turning profile has no region with $s_w = 1$ the secondary drainage profile doesn't have one either. This is illustrated by the pair $S_w = 0.15$, $S^t = 0.2$. The relevant relation hence is $Z_1^{id}(S_w, S^t)$. For intermediate turning saturations, e.g. here $S^t = 0.5$, which have a region with $s_w = 1$ the secondary drainage profile may lose that region in the transition zone as illustrated by the profile for a saturation $S_w = 0.4$. The transition relation is therefore expressed for smaller saturations S_w by $Z_1^{id}(S_w, S^t)$ and for bigger saturations by $Z_2^{id}(S_w, S^t)$. For large turning saturations, here e.g. $S^t = 0.8$ with the example $S_w = 0.7$ secondary drainage profile, $z^* > 1$ and hence the transition from primary imbibition to primary drainage is completed before the region with $s_w = 1$ vanishes in the column. The complete transition relation is therefore expressed by $Z_3^{id}(S_w, S^t)$.

The bounds are again expressed in saturations. For the secondary drainage, the upper bound

$$\bar{S}_u^{id}(S^t) = S^t \quad (68)$$

is trivial but the lower bound has three branches according to the three cases illustrated in Fig. 4. These consist of either using $Z_1^i(S^t)$ or $Z_2^i(S^t)$ to obtain z^t from S^t and $S_1^d(\bar{z}_\ell^{id})$ or $S_2^d(\bar{z}_\ell^{id})$ to obtain \bar{S}_ℓ^{id} from \bar{z}_ℓ^{id} of eq. (60). Again the combination $Z_1^i - S_2^d$ is not possible. Explicitly, this is given by

$$\bar{S}_\ell^{id}(S^t) = \begin{cases} S_1^d \left(\bar{z}_\ell^{id} \left[Z_1^i(S^t) \right] \right), & S^t < \frac{\Pi}{\Pi+B}, \\ S_1^d \left(\bar{z}_\ell^{id} \left[Z_2^i(S^t) \right] \right), & \bar{S}_1^{id} \geq S^t \geq \frac{\Pi}{\Pi+B}, \\ S_2^d \left(\bar{z}_\ell^{id} \left[Z_2^i(S^t) \right] \right), & S^t > \bar{S}_1^{id}, \end{cases} \quad (69)$$

where \bar{S}_1^{id} defines the turning saturation above which the transition from primary imbibition to primary drainage happens before \bar{z}_1^{id} leaves the reservoir. Hence, it is given as

$$\begin{aligned} \bar{S}_1^{id} : \quad & z^* \left[Z_1^d \left(\frac{1}{1+B} \right), Z_2^i(\bar{S}_1^{id}) \right] = 1 \\ \Rightarrow \bar{S}_1^{id} = & \frac{1+B-B\Pi}{1+B}. \end{aligned} \quad (70)$$

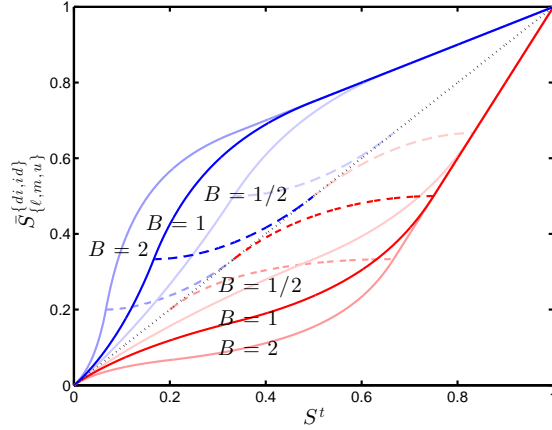


Fig. 8 Illustration of the transition region between the two primary curves for a secondary imbibition (blue curves) and a secondary drainage (red curves). The solid curves show $\bar{S}_u^{di}(S^t)$ and $\bar{S}_\ell^{id}(S^t)$. The dashed curves show $\bar{S}_m^{di}(S^t)$ respectively $\bar{S}_m^{id}(S^t)$. The dark curves correspond to $B = 1$, brighter curves show $B = 2$ and $B = \frac{1}{2}$ (labels over the solid curves).

For intermediate turning saturations (second case in eq. (69)) the position \bar{z}_1^{id} passes 0 in the transition zone. The corresponding saturation is

$$\bar{S}_m^{id}(S^t) = S_1^{id} \left[-\frac{1}{B}, Z_2^i(S^t) \right]. \quad (71)$$

Finally, the position of the vanishing capillary pressure is expressed in terms of saturations as

$$Z^{id}(S_w, S^t) = \begin{cases} Z^d(S_w), & S_w < \bar{S}_\ell^{id}(S^t), \\ Z_T^{id}(S_w, S^t), & \bar{S}_\ell^{id}(S^t) \leq S_w < \bar{S}_u^{id}(S^t), \\ Z^i(S_w), & \bar{S}_u^{id}(S^t) \leq S_w \end{cases} \quad (72)$$

where the transition zone function is given by

$$Z_T^{id}(S_w, S^t) = \begin{cases} Z_1^{id}(S_w, S^t), & S^t < \frac{\Pi}{\Pi+B}, \\ \begin{cases} Z_2^{id}(S_w, S^t), & S_w < \bar{S}_m^{id}(S^t), \\ Z_3^{id}(S_w, S^t), & S_w \geq \bar{S}_m^{id}(S^t), \end{cases} & \frac{\Pi}{\Pi+B} \leq S^t < \bar{S}_1^{id}, \\ Z_3^{id}(S_w, S^t), & \bar{S}_1^{id} \leq S^t. \end{cases} \quad (73)$$

Figure 8 illustrates the bounds $\bar{S}_\ell^{id}(S^t)$ and $\bar{S}_m^{id}(S^t)$ of the transition zone for the secondary drainage (red curves) and also $\bar{S}_u^{di}(S^t)$ and $\bar{S}_m^{di}(S^t)$ for the secondary imbibition (blue curves). Two things can be learned from this figure. First, independent of B the size of the transition zone vanishes at large and small saturations for drainage and imbibition. Second, for large B the linear branch for large turning saturations dominates. This suggests a possible simplification: For sufficiently large B the saturation at the end of the transition zone could be approximated only by

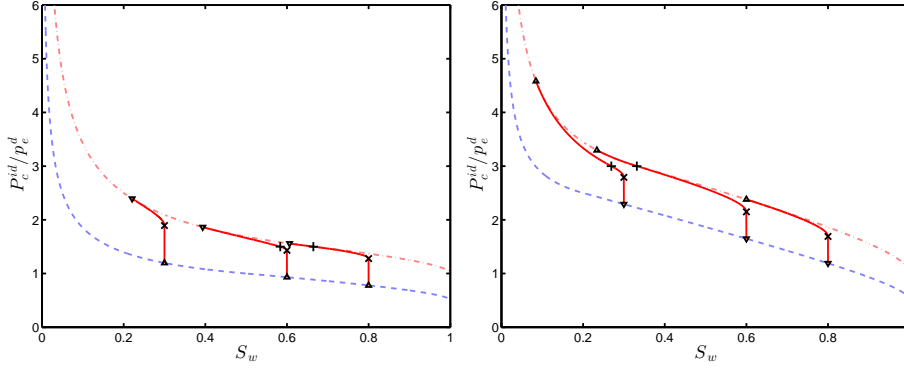


Fig. 9 The transition part (solid red curves) of the coarse-scale capillary pressure – coarse-scale saturation relation for a secondary drainage for example turning saturations $S^t = \{0.3, 0.6, 0.8\}$, $B = \frac{1}{2}$ (left) and $B = 2$ (right) and $\Pi = \frac{1}{2}$. The bounding primary imbibition curves are shown as dashed blue and the bounding primary drainage curves as dash-dotted red curves. The values $P_c^i(S^t)$ are shown as upwards pointing triangles, the values $P_c^{id}(S^t, S^t)$ as crosses, $P_c^{id}(\bar{S}_\ell^{id}(S^t), S^t)$ as downwards pointing triangles and $P_c^{id}(\bar{S}_m^{id}(S^t), S^t)$ as pluses.

the linear branch. In combination with a linear interpolation between the values on the primary curves for the bounding saturations the terms would simplify substantially. The model might even give better results because it compensates the too simplistic approach to hysteresis on the fine-scale.

The jump $\Delta z^{id} = z^t - \bar{z}_u^{id}(z^t)$ in terms of turning saturation is obtained from eq. (61) and is given by

$$\Delta z^{id}(S^t) = \begin{cases} \frac{\Pi-1}{\Pi} Z_1^i(S^t), & S^t \leq \frac{\Pi}{B+\Pi}, \\ \frac{1-\Pi}{B}, & S^t > \frac{\Pi}{B+\Pi}. \end{cases} \quad (74)$$

The limit of the fraction for $B \rightarrow \infty$ of this difference with respect to the difference between the main loops is hence identical with the secondary imbibition.

Coarse parameter functions

Given Z^{id} , the capillary pressure, identical to eq. (28), can be written as

$$P_c^{id}(S_w, S^t) = p_e^d B \left(1 - Z^{id}(S_w, S^t) \right). \quad (75)$$

Figure 9 illustrates the relationship for $B = \frac{1}{2}$ (left) and $B = 2$ (right) for the secondary drainage similar to Fig. 5 for secondary imbibition. Here the transition zone is shown for three example turning saturations as red solid curves. Starting from the turning saturation (upwards pointing triangle) on the primary imbibition curve the capillary pressure increases without a change in saturation until the value $P_c^{id}(S^t, S^t)$ is reached (crosses). The transition curve approaches the primary drainage curve and hits it at $\bar{S}_\ell^{id}(S^t)$ (downwards pointing triangles). If the transition zone includes a transition from Z_2^{id} to Z_3^{id} at \bar{S}_m^{id} (this is the case for $S^t = 0.6$ and $S^t = 0.8$ at $B = \frac{1}{2}$ and $S^t = 0.6$ at $B = 2$) the corresponding value $P_c^{id}(\bar{S}_m^{id})$ is shown by a plus.

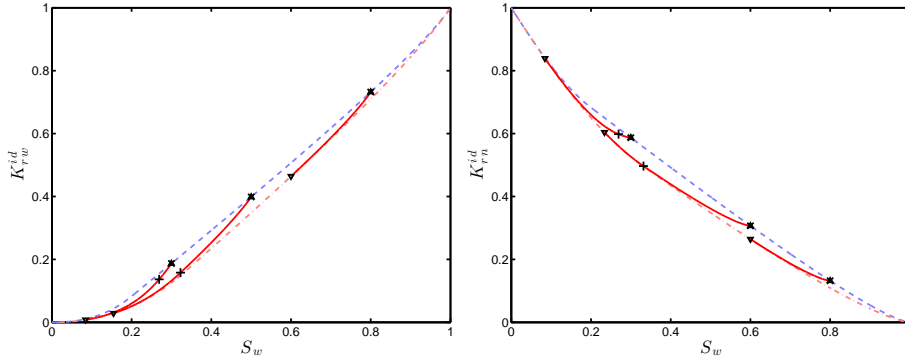


Fig. 10 The transition part (solid red curves) of the coarse-scale wetting relative permeability (left) – and non-wetting relative permeability (right) – coarse-scale saturation relation for a secondary imbibition for example turning saturations $S^t = \{0.3, 0.6, 0.8\}$, $B = 2$ and $\Pi = \frac{1}{2}$. The bounding primary imbibition curves are shown as dashed blue and the bounding primary drainage curves as dash-dotted red curves. The values $K_{r\alpha}^i(S^t)$ are shown as upwards pointing triangles, the coinciding values $K_{r\alpha}^{id}(S^t, S^t)$ as crosses, $K_{r\alpha}^{id}(\bar{S}_\ell^{id}(S^t), S^t)$ as downwards pointing triangles and $K_{r\alpha}^{id}(\bar{S}_m^{id}(S^t), S^t)$ as pluses.

The relative permeabilities are again obtained similar to the coarse-scale saturation in terms of z_0 and z^t . For the secondary drainage the transition-zone relative permeability $K_{r\alpha T}^{id}$ is given by

$$K_{r\alpha T}^{id}(S_w, S^t) = \begin{cases} K_{r\alpha 1}^{id}(S_w, S^t), & S^t < \frac{\Pi}{\Pi+B}, \\ \begin{cases} K_{r\alpha 2}^{id}(S_w, S^t), & S_w < \bar{S}_m^{id}(S^t), \\ K_{r\alpha 3}^{id}(S_w, S^t), & S_w \geq \bar{S}_m^{id}(S^t), \end{cases} & \frac{\Pi}{\Pi+B} \leq S^t < \bar{S}_1^{id}, \\ K_{r\alpha 3}^{id}(S_w, S^t), & \bar{S}_1^{id} \leq S^t \end{cases} \quad (76)$$

with the same branches as in eq. (72) and (75) and $\alpha \in \{w, n\}$. These branches yield integration boundaries for the upscaling procedure. Explicitly the integrals are given by

$$K_{r\alpha 1}^{id}(S_w, S^t) = \int_0^{z^*} k_{r\alpha} \left(s_1^d \left[z, Z_1^{id}(S_w, S^t) \right] \right) dz + \int_{z^*}^1 k_{r\alpha} \left(s_1^i \left[z, Z_1^i(S^t) \right] \right) dz \quad (77)$$

where the arguments of $z^* = z^* \left[Z_1^{id}(S_w, S^t), Z_1^i(S^t) \right]$ have been omitted and

$$K_{r\alpha 2}^{id}(S_w, S^t) = \int_0^{z^*} k_{r\alpha} \left(s_1^d \left[z, Z_2^{id}(S_w, S^t) \right] \right) dz + \int_{z^*}^1 k_{r\alpha} \left(s_1^i \left[z, Z_2^i(S^t) \right] \right) dz \quad (78)$$

where the arguments of $z^* = z^* [Z_2^{id}(S_w, S^t), Z_2^i(S^t)]$ have been omitted and

$$K_{r\alpha 3}^{id}(S_w, S^t) = \bar{z}_1^{id} k_{r\alpha}(1) + \int_{\bar{z}_1^{id}}^{z^*} k_{r\alpha} \left(s_1^d [z, Z_3^{id}(S_w, S^t)] \right) dz + \int_{z^*}^1 k_{r\alpha} \left(s_1^i [z, Z_2^i(S^t)] \right) dz \quad (79)$$

where the arguments of $z^* = z^* [Z_3^{id}(S_w, S^t), Z_2^i(S^t)]$ and $\bar{z}_1^{id} = \bar{z}_1^{id} [Z_3^{id}(S_w, S^t)]$ have been omitted.

Figure 10 illustrates the relative permeability for the wetting phase (left) and the non-wetting phase (right) for a secondary drainage with $B = 2$ similar to Fig. 6 for the secondary imbibition. The transition zone is shown for three example turning saturations as red solid curves. The values $K_{r\alpha}^i(S^t)$ and $K_{r\alpha}^{id}(\bar{S}_u^{id}(S^t), S^t)$ coincide and crosses and upwards pointing triangles are on top of each other. The transition leaves the imbibition curve with a substantial kink and approaches the primary drainage curve smoothly and hits it at $\bar{S}_\ell^{id}(S^t)$ (downwards pointing triangles). The transition zone includes a transition from Z_2^{id} to Z_3^{id} at \bar{S}_m^{id} for $S^t = 0.3$ and $S^t = 0.6$. The corresponding values $K_{rw}^{id}(\bar{S}_m^{id})$ and $K_{rn}^{id}(\bar{S}_m^{id})$ are shown by pluses.

4 Summary

We have derived explicit analytic expressions for vertically integrated capillary pressure and relative permeability functions for primary and secondary drainage and imbibition for a Brooks-Corey fine-scale capillary pressure relation with pore-size distribution index $\lambda = 2$ and quadratic fine-scale relative permeabilities. These functions are particularly helpful for analytical studies with vertically integrated models which include the capillary fringe. The impact of the differences of a drainage and imbibition parametrization has been studied in particular for the relative permeabilities because of its non-monotonic behavior with respect to the ratio between buoyancy and capillary forces B .

Appendix

Limits of capillary pressure relations for primary processes

For $B \rightarrow 0$ the branch $Z_1^X(S_w)$ is relevant. Hence, for the limit $\lim_{B \rightarrow 0} P_c^X$ we write

$$P_c^X(S_w) = p_c^d B \left[1 - \frac{1}{2} \left(1 - \sqrt{1 + \frac{4\Gamma^2}{B^2 S_w}} \right) \right] = \frac{p_c^d}{2} \left(B + \sqrt{B^2 + \frac{4\Gamma^2}{S_w}} \right) \stackrel{B \rightarrow 0}{=} p_c^X(S_w), \quad (80)$$

where first the square root was approximated by its Taylor expansion and in the second approximation terms of order B and higher have been neglected.

For $B \rightarrow \infty$ the branch $Z_2^X(S_w)$ is relevant. Therefore we write for the limit $\lim_{B \rightarrow \infty} P_c^X$

$$\begin{aligned} P_c^X(S_w) &= p_e^d B \left(1 - \frac{1+S_w}{2} + \frac{\Gamma}{B} + \sqrt{\frac{4\Gamma+B}{4B} - \frac{2\Gamma+B}{2B} S_w + \frac{S_w^2}{4}} \right) \\ &= p_e^d \left[\frac{B}{2}(1-S_w) + \Gamma + \frac{B}{2}(1-S_w) \sqrt{1 + \frac{4\Gamma}{B} \frac{1}{1-S_w}} \right] \\ &\stackrel{B \gg 1}{\approx} p_e^d \left[\frac{B}{2}(1-S_w) + \Gamma + \frac{B}{2}(1-S_w) \left(1 + \frac{2\Gamma}{B} \frac{1}{1-S_w} \right) \right] = p_e^d [B(1-S_w) + 2\Gamma], \end{aligned} \quad (81)$$

where the square root was approximated by its Taylor expansion. From eq. (81) we immediately obtain the limit of the difference between drainage and imbibition as

$$\lim_{B \rightarrow \infty} P_c^d(S_w) - P_c^i(S_w) = 2p_e^d(1 - \Pi). \quad (82)$$

Explicit expressions for secondary processes

Explicit analytic expressions for the relationship between coarse scale saturations and the position of vanishing fine-scale capillary pressure are given.

Drainage followed by an imbibition

The three functions for the position of the vanishing capillary pressure for a drainage followed by an imbibition are given by

$$\begin{aligned} Z_1^{di}(S_w, S^t) &= \frac{1}{2B^2 S_w (Z_1^d - 1) - 2} \left[2\Pi - 1 - (2\Pi + B^2 S_w) Z_1^d + B^2 S_w Z_1^{d^2} \right. \\ &\quad \left. - \sqrt{B^2 S_w (Z_1^d - 1) Z_1^d - 1} \right. \\ &\quad \left. \sqrt{4(\Pi^2 - \Pi)(Z_1^d - 1) - 1 + B^2 S_w (Z_1^d - 1) Z_1^d} \right] \end{aligned} \quad (83)$$

and

$$\begin{aligned} Z_2^{di}(S_w, S^t) &= \frac{1}{2(B^2 Z_1^d - B^2)} \left[2B\Pi - 1 - B^2 S_w + (B^2 S_w - B^2 - 2B\Pi) Z_1^d + B^2 Z_1^{d^2} \right. \\ &\quad \left. + \sqrt{2B - 1 - B^2 S_w + (B^2 S_w - 2B + B^2) Z_1^d - B^2 Z_1^{d^2}} \right. \\ &\quad \left. \sqrt{2B(2\Pi - 1) - 1 - B^2 S_w + (2B + B^2 - 4B\Pi + B^2 S_w) Z_1^d - B^2 Z_1^{d^2}} \right] \end{aligned} \quad (84)$$

and

$$\begin{aligned} Z_3^{di}(S_w, S^t) &= \frac{1}{2(B^2 Z_2^d - B^2)} \left[2B\Pi - 1 - B^2 S_w + (B^2 S_w - B^2 - 2B\Pi) Z_2^d + B^2 Z_2^{d^2} \right. \\ &\quad \left. + \sqrt{2B - 1 - B^2 S_w + (B^2 S_w - 2B + B^2) Z_2^d - B^2 Z_2^{d^2}} \right. \\ &\quad \left. \sqrt{2B(2\Pi - 1) - 1 - B^2 S_w + (2B + B^2 - 4B\Pi + B^2 S_w) Z_2^d - B^2 Z_2^{d^2}} \right]. \end{aligned} \quad (85)$$

In eq. (83) and (84) the argument of $Z_1^d = Z_1^d(S^t)$ and in eq. (85) the argument of $Z_2^d = Z_2^d(S^t)$ have been omitted to improve the readability.

Imbibition followed by a drainage

The three functions for the position of the vanishing capillary pressure for an imbibition followed by a drainage are given by

$$Z_1^{id}(S_w, S^t) = \frac{1}{2[\Pi^2 - B^2 S_w (Z_1^i - 1)]} \left[\Pi^2 - 2\Pi + (2\Pi + B^2 S_w) Z_1^i - B^2 S_w Z_1^{i2} \right. \\ \left. - \sqrt{4[B^2 S_w (Z_1^i - 1) - \Pi^2](Z_1^i - 1) Z_1^i + [\Pi^2 + 2\Pi(Z_1^i - 1) - B^2 S_w (Z_1^i - 1) Z_1^i]^2} \right] \quad (86)$$

and

$$Z_2^{id}(S_w, S^t) = \frac{1}{2[\Pi^2 - B^2 S_w (Z_2^i - 1)]} \left[\Pi^2 - 2\Pi + (2\Pi + B^2 S_w) Z_2^i - B^2 S_w Z_2^{i2} \right. \\ \left. - \sqrt{4[B^2 S_w (Z_2^i - 1) - \Pi^2](Z_2^i - 1) Z_2^i + [\Pi^2 + 2\Pi(Z_2^i - 1) - B^2 S_w (Z_2^i - 1) Z_2^i]^2} \right] \quad (87)$$

and

$$Z_3^{id}(S_w, S^t) = \frac{1}{2(B^2 Z_2^i - B^2)} \left[2B - \Pi^2 - B^2 S_w + (B^2 S_w - 2B - B^2) Z_2^i + B^2 Z_2^{i2} \right. \\ \left. + \left(\left[\Pi^2 - 2B + B^2 S_w + (2B + B^2 - B^2 S_w) Z_2^i - B^2 Z_2^{i2} \right]^2 - 4[B^2 Z_2^i - B^2] \right. \right. \\ \left. \left. \times \left[2\Pi - 1 - \Pi^2 + (1 - 2\Pi + 2B - B^2 S_w) Z_2^i + (B^2 S_w - 2B) Z_2^{i2} \right] \right)^{\frac{1}{2}} \right]. \quad (88)$$

In eq. (86) the argument of $Z_1^i = Z_1^i(S^t)$ and in eq. (87) and (88) the argument of $Z_2^i = Z_2^i(S^t)$ have been omitted to improve the readability.

References

1. Bear, J.: Dynamics of Fluids in Porous Media. Dover Publications, New York (1972)
2. Beliaev, A.Y., Hassanizadeh, S.M.: A theoretical model of hysteresis and dynamic effects in the capillary relation for two-phase flow in porous media. *Transport in Porous Media* **43**, 487–510 (2001)
3. Brooks, R.H., Corey, A.T.: Hydraulic properties of porous media. In: *Hydrol. Pap.*, vol. 3. Colorado State University, Fort Collins (1964)
4. Court, B., Bandilla, K.W., Celia, Michael A., Janzen, A., Dobossy, M., Nordbotten, J.M.: Applicability of vertical-equilibrium and sharp-interface assumptions in CO_2 sequestration modeling. submitted (2012)
5. Cueto-Felgueroso, L., Juanes, R.: Nonlocal interface dynamics and pattern formation in gravity-driven unsaturated flow through porous media. *Physical Review Letters* **101**(24), 244504 (2008). DOI 10.1103/PhysRevLett.101.244504. URL <http://link.aps.org/abstract/PRL/v101/e244504>
6. Doster, F., Nordbotten, J., Celia, M.: Impact of capillary hysteresis and trapping on vertically integrated models for CO_2 storage. in preparation (2012)
7. Doster, F., Zegeling, P.A., Hilfer, R.: Numerical solutions of a generalized theory for macroscopic capillarity. *Phys. Rev. E* **81**(3), 036307 (2010). DOI 10.1103/PhysRevE.81.036307
8. Gasda, S.E., Nordbotten, J.M., Celia, M.A.: Vertical equilibrium with sub-scale analytical methods for geological CO_2 sequestration. *COMPUTATIONAL GEOSCIENCES* **13**(4), 469–481 (2009). DOI 10.1007/s10596-009-9138-x
9. Hassanizadeh, S., Celia, M.A., Dahle, H.: Dynamic effect in the capillary pressure-saturation relationship and its impacts unsaturated flow. *Vadose Zone Journal* **1**, 38–57 (2002)

10. Hesse, M., Tchelepi, H., Cantwell, B., Orr Jr., F.: Gravity currents in horizontal porous layers: transition from early to late self-similarity. *J. Fluid Mech.* **577**, 363–383 (2007)
11. Joekar, V., Hassanizadeh, S.M., Leijnse, A.: Insights into the relationships among capillary pressure, saturation, interfacial area and relative permeability using pore-scale network modeling. *Transport in Porous Media* **74**(2), 201219 (2008)
12. Juanes, R., MacMinn, C., Szulczewski, M.: The footprint of the CO₂ plume during carbon dioxide storage in saline aquifers: Storage efficiency for capillary trapping at the basin scale. *Transport in Porous Media* **82**, 19–30 (2010). URL <http://dx.doi.org/10.1007/s11242-009-9420-3>. DOI 10.1007/s11242-009-9420-3
13. Lake, L.W.: *Enhanced Oil Recovery*. Prentice Hall, New Jersey (1989)
14. Morrow, N.R., Harris, C.C.: Capillary equilibrium in porous materials. *Soc. Pet. Eng. Jour.* pp. 15 – 24 (1965)
15. Nordbotten, J., Celia, M.: *Geological Storage of CO₂* (2011)
16. Nordbotten, J., Dahle, H.: Impact of Capillary Forces on Large-Scale Migration of CO₂. In: 18th Conference on Computational Methods for Water Resources. Barcelona, Spain (2010). URL [//arks.princeton.edu/ark:/88435/dsp01pn89d657garks.princeton.edu/ark:/88435/dsp01f7623c57k](http://arks.princeton.edu/ark:/88435/dsp01pn89d657garks.princeton.edu/ark:/88435/dsp01f7623c57k)
17. Nordbotten, J.M., Celia, M.A.: An improved analytical solution for interface up-coning around a well. *WATER RESOURCES RESEARCH* **42**(8) (2006). DOI 10.1029/2005WR004738
18. Nordbotten, J.M., Celia, M.A.: Similarity solutions for fluid injection into confined aquifers. *Journal of Fluid Mechanics* **561**, 307–327 (2006). DOI 10.1017/S0022112006000802
19. Nordbotten, J.M., Dahle, H.K.: Impact of the capillary fringe in vertically integrated models for CO(2) storage. *WATER RESOURCES RESEARCH* **47** (2011). DOI 10.1029/2009WR008958
20. Yortsos, Y.C.: A theoretical analysis of vertical flow equilibrium **18**, 107–129 (1995)